

Numerical simulation of deflagration-to-detonation transition via shock-multiple flame kernels interactions

Georgios Bakalis ^a, Kelsey C. Tang-Yuk ^b, Xiaocheng Mi ^c, Nikos Nikiforakis ^c and Hoi Dick Ng ^{a†}

^a Department of Mechanical, Industrial and Aerospace Engineering, Concordia University,
Montréal, QC, H3G 1M8, Canada

^b Department of Mechanical Engineering, McGill University, Montréal, QC, H3A 0C3, Canada

^c Cavendish Laboratory, Department of Physics, University of Cambridge, Cambridge, CB3
0HE, UK

[†]Corresponding Author

Department of Mechanical, Industrial and Aerospace Engineering
Concordia University
Montréal, QC H3G 1M8, Canada
e-mail: hoing@encs.concordia.ca
Tel.: 1 (514) 848-2424 ext. 3177
Fax: 1 (514) 848-3175

Conflicts of Interest: The authors declare no conflict of interest.

Final manuscript submitted to *Computers & Mathematics with Applications*
(SI: Numerical Fluids 2018)

April 2020

Numerical simulation of deflagration-to-detonation transition via shock-multiple flame kernels interactions

Georgios Bakalis ^a, Kelsey C. Tang-Yuk ^b, Xiaocheng Mi ^c, Nikos Nikiforakis ^c and Hoi Dick Ng ^a

^a Department of Mechanical, Industrial and Aerospace Engineering, Concordia University, Montréal, QC, H3G 1M8, Canada

^b Department of Mechanical Engineering, McGill University, Montréal, QC, H3A 0C3, Canada

^c Cavendish Laboratory, Department of Physics, University of Cambridge, Cambridge, CB3 0HE, UK

Abstract

The deflagration-to-detonation transition via the interaction of a weak shock with a series of discrete laminar flames is analyzed computationally based on the unsteady reactive Navier-Stokes equations with one-step Arrhenius chemistry. For comparison, simulations with the Euler equations are also performed. The numerical setup aims to mimic an array of laminar flames ignited at different spark times, artificially inducing chemical activity to stimulate the coupling between the gas dynamics and the chemical energy release for the deflagration-to-detonation transition. The interaction of the weak shock with the first cylindrical flame demonstrates a very good agreement with the results in the literature and that a single weak shock-flame interaction is insufficient to cause a prompt DDT. However, a high degree of Richtmyer-Meshkov instabilities induced by repetitive shock-flame and shock-boundary interactions generate turbulence that accelerates the flame surface, referred to as the flame brush, until eventually a hot spot ignition in the unreacted material develops into a multi-headed detonation wave. In the absence of physical diffusion in the Euler simulation, the enhanced burning rate of the turbulent flame brush is suppressed. Nevertheless, the intense flow fluctuations generated by the interactions of shocks, boundary and flames create the conditions under which a deflagration-to-detonation transition can potentially occur at later times. A parametric study is also reported in this paper to assess the influence of various physical parameters on the transition event and to explore scaling relationships among these parameters.

Keywords: Detonation-to-deflagration transition; Shock-flame interaction; Propulsion; CFD

Classification Codes: 76J20, 76N15, 80A25, 76M12

1. INTRODUCTION

A gaseous detonation is a supersonic combustion-driven wave travelling at a velocity of the order of 2 km/s, across which a significant increase in pressure and temperature occurs in the medium. In recent years, pressure-gain detonative combustion attracts renewing interest due to its potential application in air-breathing hypersonic propulsion to improve the thermal efficiency of engine systems [1-5]. Generally, a detonation can be initiated in two ways. One way is by a rapid deposition of a large amount of energy into the combustible mixture, referred to as direct initiation [6]. The detonation is formed instantaneously from the decaying strong blast wave. In the limit of an ideal point source energy, the initiation energy is the sole parameter that determines whether a detonation can be initiated. This method of detonation initiation requires the use of a very powerful energy deposition, e.g., from a high-voltage capacity spark discharge, a condensed phase energetic explosive material, or laser ignition [7]. Hence, it is not practical for any realistic propulsion applications.

The other mode of detonation initiation is referred to as deflagration-to-detonation transition (DDT). The DDT phenomenon has attracted significant attention in applied research due to its potential applications in hypersonic propulsion systems such as pulse detonation engines (PDEs), as well as in industrial process safety, particularly with the recent interest in the hydrogen economy, where DDT phenomenon is the most probable cause resulting in the formation of detonations in accidental explosions [8, 9]. DDT involves an initial ignition of a combustible mixture by some relatively weak energy source producing a laminar flame, followed by an acceleration through interactions with its confinement. The generation of turbulence results in a coupled shock wave-reaction zone structure and eventually the onset of a detonation under appropriate conditions [8-11]. The distance required for the transition is referred to as the DDT or “run-up” distance.

For the successful and steady operation of detonation-based engines such as PDEs, repetitive initiation of detonation waves is required [9]. DDT is by nature a complex and stochastic process due to various turbulent and instability mechanisms that cause the transition from low-speed flame propagation to a high-speed turbulent deflagration and eventually a detonation wave. After a small spark has created a deflagration, the transition needs to cover a relatively long process towards the onset of detonation. Experiments in simple straight tubes also showed that during the acceleration of a flame to a detonation, the transition or run-up distance required for deflagration-to-detonation transition is hardly reproducible due to the aforementioned turbulent and instability mechanisms that play a role in promoting the transition to detonation [11]. Therefore, having consistent and repeatable DDT as a viable initiation method in detonation engines remains challenging. For practical purposes, particularly in propulsion applications, the key issue is to find appropriate mechanisms for rapidly generating detonation waves from DDT with a relatively weak ignition source; in other words, to reduce the time and distance required for a complete DDT process in order to minimize the size of the engineering system and the amount of energy input required for initiation, thus, producing reproducible shot-to-shot performance [9, 12]. Solving this issue will result in more efficient, compact engines which can operate with increased pulse frequency. Up-to-date, the common techniques to facilitate the flame acceleration are to modify the boundary condition by inserting a Shchelkin spiral, rectangular obstacles or by using jets to promote the generation of turbulence [11].

In the literature, a number of computational studies on the initial shock-flame and shock-boundary interactions have been performed to describe the fundamentals of a DDT process [10, 13-16]. These studies show that compressible turbulence and shock-flame interaction are responsible for creating the proper condition for the final onset of detonation. As in other

detonation phenomena, the key mechanism for a successful DDT is the close coupling between energy release and shock wave propagation [17]. In the pioneering work by Zel'dovich *et al.* [18], the coupling originated from the shock-flame and shock-boundary interaction, eventually leading to a spontaneous onset of detonation, was modeled by an initial gradient of auto-ignition delay time through temperature and composition non-uniformities in the pre-conditioned reactive mixture. Similar studies were subsequently carried out numerically and theoretically by a number of researchers (see [19] and references therein). These factors promote the amplification of a high-speed shock through coherent energy release, later termed by Lee & Moen [11, 20] as the concept of Shock Wave Amplification by Coherent Energy Release (SWACER). This concept was used to qualitatively explain the photochemical initiation and turbulent jet initiation of gaseous detonations, “explosion within the explosion” at the onset of detonation [11], and detonation formation from a temperature gradient [21, 22].

In order to promote the coherent coupling between the gas dynamics and energy release to control the transition from deflagration to detonation, an engineering concept of using spatially distributed energy release was previously proposed. The idea is to synchronize the propagation and amplification of a weak shock interacting with an array of laminar flames ignited through different spark sequences in the reactive mixture to achieve very short distances for DDT in smooth tubes. Such ideas of using external sources to facilitate the onset of a detonation was proposed as early as the 1950's by Zel'dovich & Kompaneets [23] theoretically and has been applied experimentally, notably by Frolov *et al.* [17, 24] using controlled triggering of electric ignition. The time delay of each ignition could be varied within a wide range (from 10 to 500 μ s). The energy of discharges is controlled by the voltage ranging from 1500 to 2500 V. The experimental work by Frolov *et al.* [24] has demonstrated the use of relatively weak igniters with

optimally tuned triggering times to promote detonation initiation in premixed $C_3H_8 + O_2 + 3N_2$ and stoichiometric C_3H_8 /air mixtures at distances as short as 0.6 – 0.7 m in a 2-inch diameter tube at normal initial conditions (at about the cross section CS7 shown in Fig. 1 of ref. [24]). Hu *et al.* [25] also simulated the rapid detonation initiation by sparks modelled by a high-energy region with ignition temperature but also with high ignition pressure. These studies demonstrate that the initiation technique using multiple sparks has the potential to induce DDT.

The primary objective of this work is to demonstrate numerically the possibility of deflagration-to-detonation transition resulting from multiple shock-flame interactions. As such, an ideal reactive flow model with a one-step chemistry is considered, avoiding the need of large computational resources and data interpretation. In this numerical investigation, the phenomenon is described by a relatively weak shock wave travelling along a tube filled with a reactive mixture and an array of cylindrical laminar flames ignited through different spark sequences as a means of artificially inducing chemical activity to stimulate the strong coupling required for the transition of deflagration-to-detonation. The present numerical work differs from that of Hu *et al.* [25]. The present investigation considers only weak sparks resulting only in the generation of laminar flame kernels across which the pressure remains constant. The effect of elevated pressure inside the flame kernels due to the high-voltage discharge, as in the experiments by Frolov *et al.* [24] and in the simulation by Hu *et al.* [25], are thus eliminated so that a more practical flame ignition by weak spark is modeled and investigated. The outcome of this numerical work will further solidify whether the proposed concept of using multiple weak sparks (while minimizing the input spark energy as much as possible) can be a potential approach for propulsion applications. Besides, the present investigation is an extension of the work of Khokhlov *et al.* [14-16] which analyzed the flow field resulting from the interaction between a

weak shock and a single laminar flame kernel. The possibility of deflagration-to-detonation transition resulting from multiple shock-flame interactions has not been explored. Using numerical simulations, a number of parameters are also varied to gauge their effect on the run-up distance and time to the onset of detonation. Validation testing has been performed to examine the effect of various numerical details on the key simulation results of the shock-flame interactions and the overall DDT process.

2. PROBLEM FORMULATIONS AND NUMERICAL METHODOLOGY

The reactive flow dynamics is governed by the unsteady, fully compressible Navier-Stokes equations [26, 27] coupled with a chemical reaction model:

$$\begin{aligned}
 \frac{\partial \rho}{\partial t} + \nabla \cdot (\rho \mathbf{V}) &= 0 \\
 \frac{\partial(\rho \mathbf{V}_i)}{\partial t} + \nabla \cdot (\rho \mathbf{V}_i \mathbf{V}) + \frac{\partial p}{\partial x_i} &= \nabla \cdot \tau_i \\
 \frac{\partial E}{\partial t} + \nabla \cdot ((E + p) \mathbf{V}) &= \nabla \cdot (\kappa \nabla T) + \nabla \cdot (\underline{\tau} \mathbf{V}) + \dot{\omega} Q \\
 \frac{\partial \rho \lambda}{\partial t} + \nabla \cdot (\rho \lambda \mathbf{V}) &= \nabla \cdot (\rho D \nabla \lambda) + \dot{\omega}
 \end{aligned} \tag{1}$$

where ρ is the density, $\mathbf{V} = (u, v, w)$ the velocity, E the total energy, p the pressure, λ the mass fraction of reactant across the domain, k the thermal conduction coefficient, D is the mass diffusion coefficient, $\dot{\omega}$ the reaction source term, and $\underline{\tau}$ the viscous stress tensor given by:

$$\tau_{ij} = \rho \nu \left(\frac{\partial V_i}{\partial x_j} + \frac{\partial V_j}{\partial x_i} \right) - \frac{2}{3} \rho \nu \frac{\partial V_k}{\partial x_k} \delta_{ij} \tag{2}$$

The total local energy of the system is defined as the sum of the kinetic energy and internal energy of the gas. The equation of state is that of an ideal gas and the reactive term is modelled with an Arrhenius rate law, i.e.:

$$T = \frac{pM}{\rho R} \quad E = \frac{1}{2} \rho \mathbf{V} \cdot \mathbf{V} + \frac{p}{(\gamma - 1)} \quad \dot{\omega} = -A \rho \lambda \exp\left(\frac{-E_a}{RT}\right) \tag{3}$$

The material and chemistry properties of the reactive mixture model a stoichiometric acetylene-air mixture as a single-gas approximation. The transport values of the kinematic viscosity, diffusion, and heat conduction are approximated by similar temperature dependence:

$$\nu = \nu_o \frac{T^n}{\rho} \quad D = D_o \frac{T^n}{\rho} \quad \frac{\kappa}{\rho c_p} = k_o \frac{T^n}{\rho} \quad (4)$$

with $n = 0.7$ and the specific heat $c_p = \gamma R/M(\gamma-1)$. ν_o , D_o , and k_o are constants given in Table 1. The system thus has a Lewis, Prandtl and Schmidt number to be unity. This model has been extensively tested and used for DDT problems, e.g., [10, 13-16, 28-32]. Initial conditions and other calibrated mixture model parameters are also summarized in Table 1. For the generic model used in this work, most of the combustion and chemical kinetic parameters are taken directly from the works of Khokhlov *et al.* [14, 15]. To better capture the reported flame speed and thickness of the corresponding one-dimensional laminar flame profile, the diffusive coefficient and pre-exponential constant in the rate law are updated using the Zel'dovich-Kamenetskii theory [27].

Mixture parameters	Value
Initial pressure p_o	1.33×10^4 Pa
Initial temperature T_o	293 K
Initial density ρ_o	1.58×10^{-1} kg/m ³
Flame temperature T_f	2340 K
Laminar flame speed S_l	1.4 m/s
Detonation velocity D_{CJ}	1870 m/s
Specific heat ratio γ	1.25
Molecular weight M	29
Chemical heat release Q	$35.0 RT_o/M$
Activation energy E_a	$29.3 RT_o$
Pre-exponential constant A	5×10^8 m ³ /kg-s
Transport constant $\nu_o = D_o = k_o$	2.4×10^{-7}

TABLE 1. Initial condition and mixture model Parameters (adapted from [14] and [27])

The present simulation is carried out in a two-dimensional configuration to look at the interaction of a weak shock wave and multiple cylindrically expanding flames. Solutions to the

governing equations described above, i.e., the reactive Navier-Stokes equations with single-step Arrhenius kinetics, are approximated using the finite-volume 2nd order Weighted Average Flux (WAF) scheme with an approximate HLLC Riemann solver and operating splitting for the source term [33]. The diffusive fluxes are evaluated using a second-order accurate finite-difference scheme. The CFL number used in the computation is 0.90. As shown in Fig. 1, adaptive mesh refinement (AMR) is employed to dynamically increase the resolution of a simulation where patches of higher grid density are laid over the coarser grids in regions of interest around shocks, flame fronts and regions of large gradients in density using a hierarchical grid structure first proposed by Berger & Oliger [34]. The AMR method refines sub-grids in time as well as in space, which allows for the numerical method to be invoked at its optimal time-step on each grid, minimizing the accumulation of truncation errors caused by sub-optimal time-stepping. Re-mapping between grids at different levels is performed by interpolation with flux corrections applied along the edge of each of the refined grids to maintain conservation [35]. To flag regions where the grid refinement is required, the following indicator function is used:

$$\sqrt{\left(\frac{\rho_{i+1,j} - \rho_{i-1,j}}{x_{i+1} - x_{i-1}}\right)^2 + \left(\frac{\rho_{i,j+1} - \rho_{i,j-1}}{y_{i+1} - y_{i-1}}\right)^2} / \rho_{i,j} > \varepsilon$$

The normalized density gradient is used to provide a measure of the total error produced by running the simulation at coarser resolution locally. ε represents a threshold which can be tuned to reduce the numerical error of the simulation at the expense of more of the simulation domain being covered with refined meshes. A value of $\varepsilon = 20$ is specified throughout. The combined AMR framework, flow and reactive source solvers has been validated for a variety of inert shock-tube problems, together with a reactive problem with exact solution, e.g., [26, 27, 36, 37].

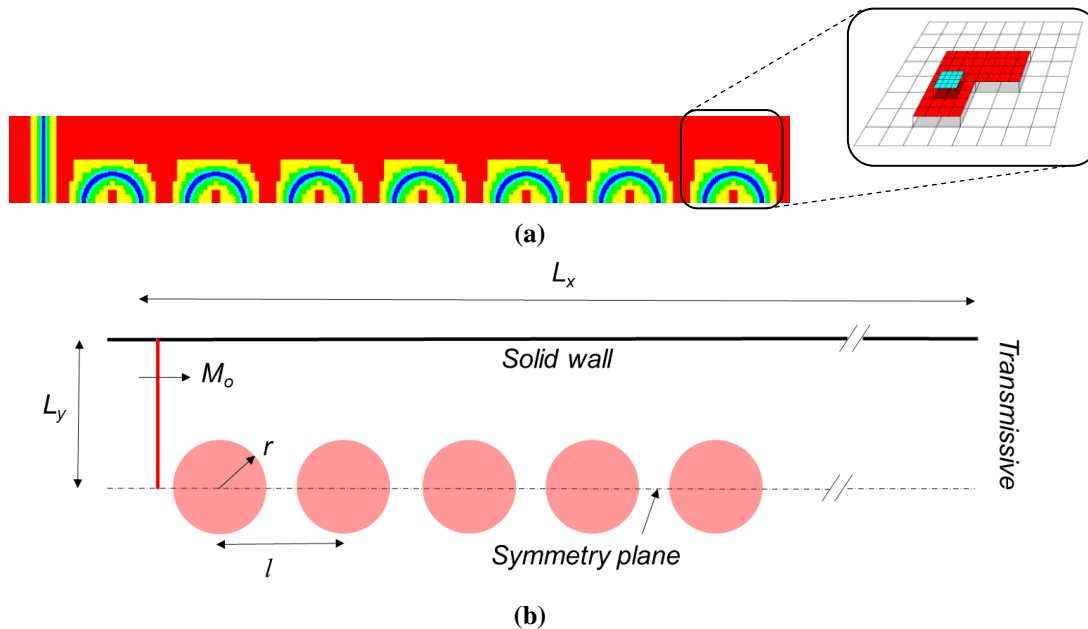


FIGURE 1. Schematic of the computational setup for the two-dimensional simulation

A schematic of the computational setup for the present two-dimensional simulations is shown in Fig. 1 with a computational domain denoted by $L_x \times L_y$, an initial flame radius r , incident shock Mach number M_o , and distance between discrete flames l . The circles shown in Fig. 1 represent initial flame kernels ignited before the shock passage. These flame kernels are embedded in the computational domain to approximate a sequence of low energy ignitions. For simplicity, these are initially set up as a discontinuity between cold reactants and hot products at constant pressure and adiabatic flame temperature T_f . The simulation is restricted to half of the domain, with a symmetry plane or reflective boundary condition applied along the lower boundary to minimize the computational expense. The top boundary is a non-slip, adiabatic, solid wall for the Navier-Stokes computation (and slip boundary condition for the Euler simulations). The left and right boundaries have transmissive, non-reflecting condition where the ghost cells take the lowest-order extrapolation of the adjacent cell values. Unless specified otherwise, five levels of AMR grid refinement are used (2, 2, 2, 2, 2). The base resolution

combined with AMR gives an effective resolution with Δx in the highest level equal to $47 \mu\text{m}$ (equivalent to approximately 5 cells across the initial flame thickness of $2.5 \times 10^{-4} \text{ m}$ or 10 cells within the 1-D detonation thickness of $\approx 0.5 \times 10^{-4} \text{ m}$).

For an initial case, 12 flame kernels were first considered to approximate a sequence of low energy ignitions in a computational domain with height $L_y = 16.5 \text{ mm}$ and length $L_x = 0.36 \text{ m}$. The choice is similar to the number of lateral ports for electrical igniters used experimentally in Frolov *et al.* [24]. The flame kernels were evenly spaced, separated by a distance of $l = 18 \text{ mm}$ from each other (center to center). Again recall that these flame kernels represent low energy ignitions and the flame surface is initially set as a discontinuity between the cold reactants outside the kernel and combustion products at adiabatic flame temperature T_f inside the flame kernel with the same initial pressure. The initial radius of the kernels, or flame amplitude, was set to $r = 4.5 \text{ mm}$. The first kernel is located at a distance $l_2 = 9 \text{ mm}$ from the left boundary. A weak planar shock which has a velocity equal to $M_o = 1.8$ is placed upstream of the first kernel, at a distance $l_1 = 6 \text{ mm}$ from the left boundary. Downstream of the shock the flow speed is set everywhere as zero, whereas upstream of the shock the flow properties are determined by the Rankine-Hugoniot condition.

3. RESULTS AND DISCUSSION

3.1 Detailed flow features and DDT via shock-multiple flames-boundary interactions

The results from the simulations are presented using temperature, pressure contours and density-schlieren plots. Here, the schlieren plots are used to provide visual identification of shocks, contact surfaces, and rarefaction waves within the flow and can be modeled numerically using the formula:

(5)

$$\varphi = \exp\left\{-\epsilon \frac{|\nabla\rho|}{\max(|\nabla\rho|)}\right\}$$

where ϵ is an amplification factor for small gradients ranging from 20 to 100.

Figure 2 first shows the early evolution of the incident weak shock after interaction with the first few discrete flames. The shock interaction with the first flame kernel leads to the distortion of its flame front as a result of the Richtmyer-Meshkov instability, occurring due to the shock acceleration of two fluids with different densities [38-43]. Due to the vorticity generated on the edges of the flame as a result of its increased angle of interaction with the shock, the flame elongates and the instability also leads to the formation of a funnel of unburned reactants intruding into the hot burned region of the flame bubble.

The schlieren plots of Fig. 2 show that after the incident shock reaches the flame kernel, the top part continues to propagate downstream outside the kernel, whereas the bottom part of the shock is partially diffracted inside the kernel and partially reflected as a circular wave. Around the surface of the bubble as shown in the first four schlieren frames, the initially planar shock is bent due to an acoustic impedance mismatch. Both the transmitted and incident shock waves are deformed through diffraction and refraction, respectively. A portion of the circular wave is reflected upstream as a rarefaction wave and the rest, after it reflects at the top boundary, either travels perpendicular to the initial shock or merges with the amplifying shock wave. Inside the flame kernel, the shock travels at a higher speed compared to the top part, and after multiple reflections and diffractions, a shock emerges from the right side of the bubble, followed by subsequent faster waves that join the leading wave and further amplify its strength. This is evident by the pressure increase behind the leading shock at later times in the pressure plots of Fig. 2. In the following collision, the funnel penetrates into the subsequent flame and pushes the

interface ahead. Similar shock reflections and diffractions repeat for all the subsequent kernels as they interact with the leading shock.

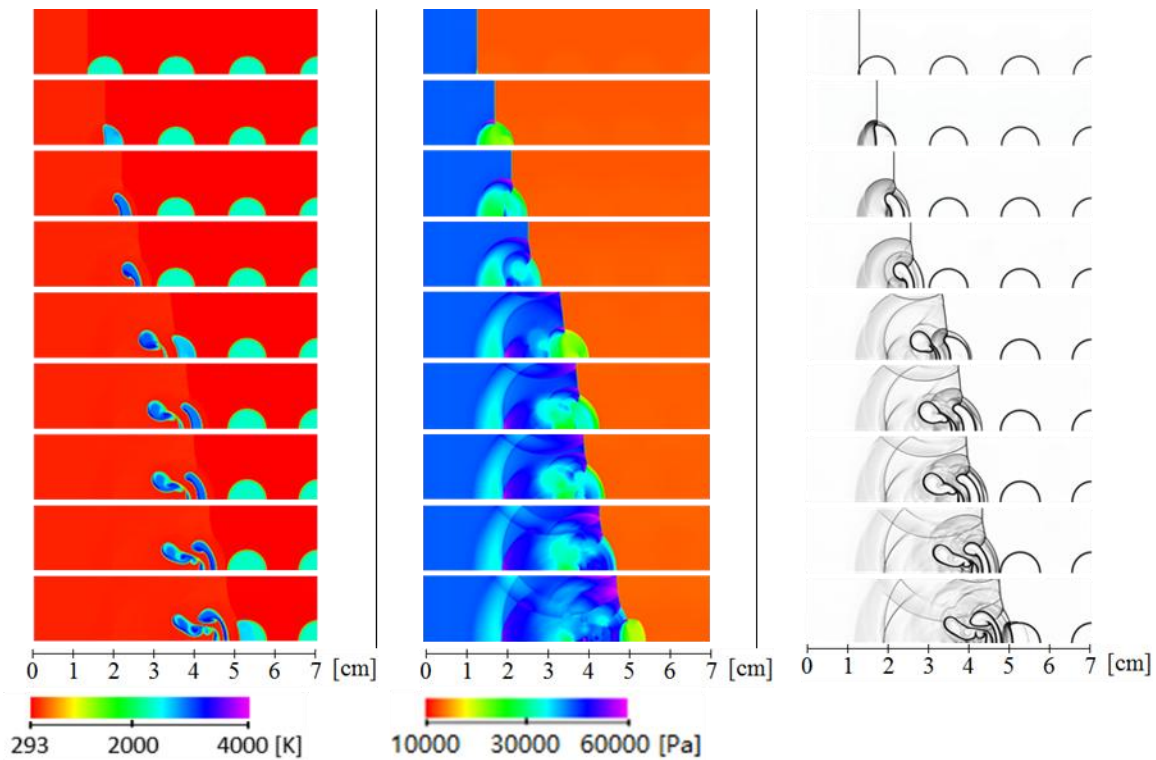


FIGURE 2. Temperature, pressure contours and schlieren plots showing the early shock-flame interactions

The shock wave proceeds to interact with the rest of the flame kernels, leading to intense mixing, turbulence and coalescence of flames to form a larger flame brush. The flame surface gradually increases, and along with an increased generation of turbulence, leads to a greater rate of energy release. A more rapid energy release accelerates the flame propagation and the transition to a turbulent flame. In order for a successful DDT to occur, the flame brush has to continue to accelerate, until achieving a critical deflagration speed, leading to an abrupt change of the mode of reaction wave propagation.

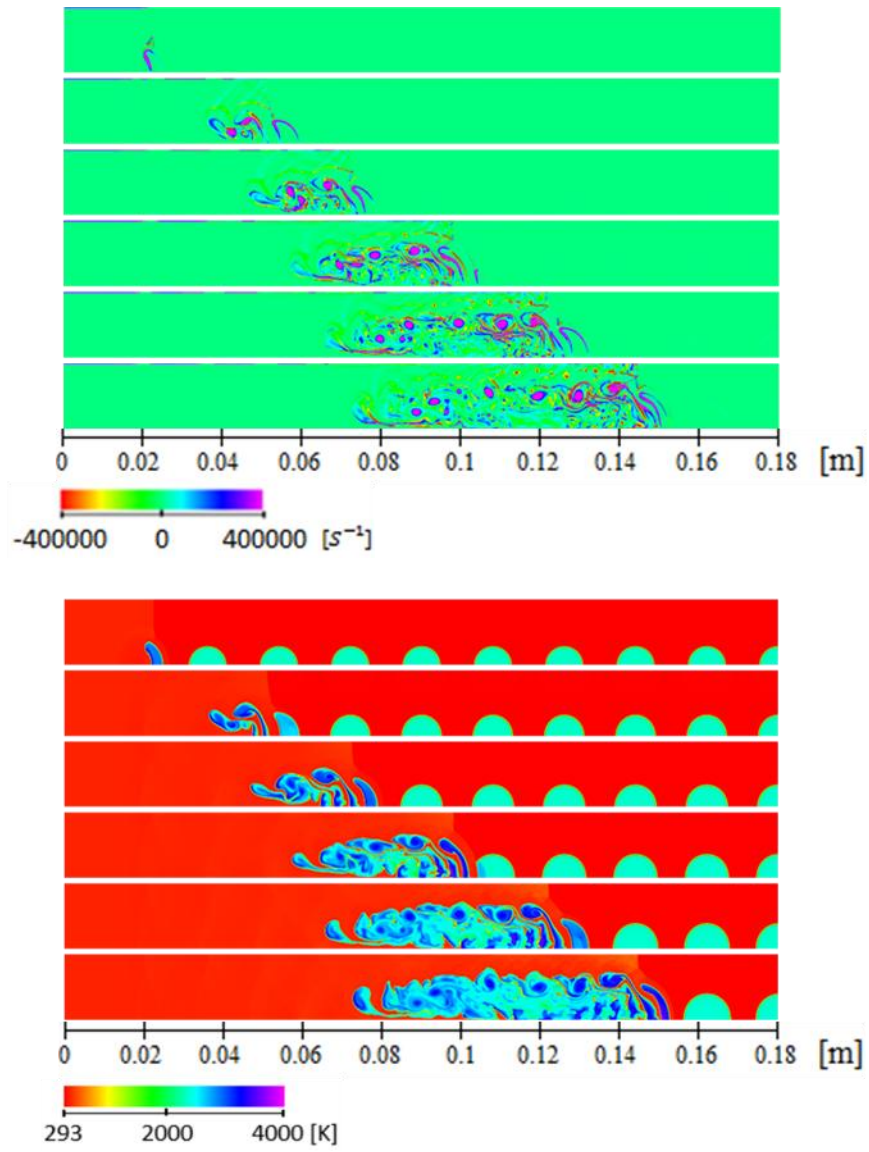


FIGURE 3. Vorticity and temperature flow fields after multiple shock-flame interactions

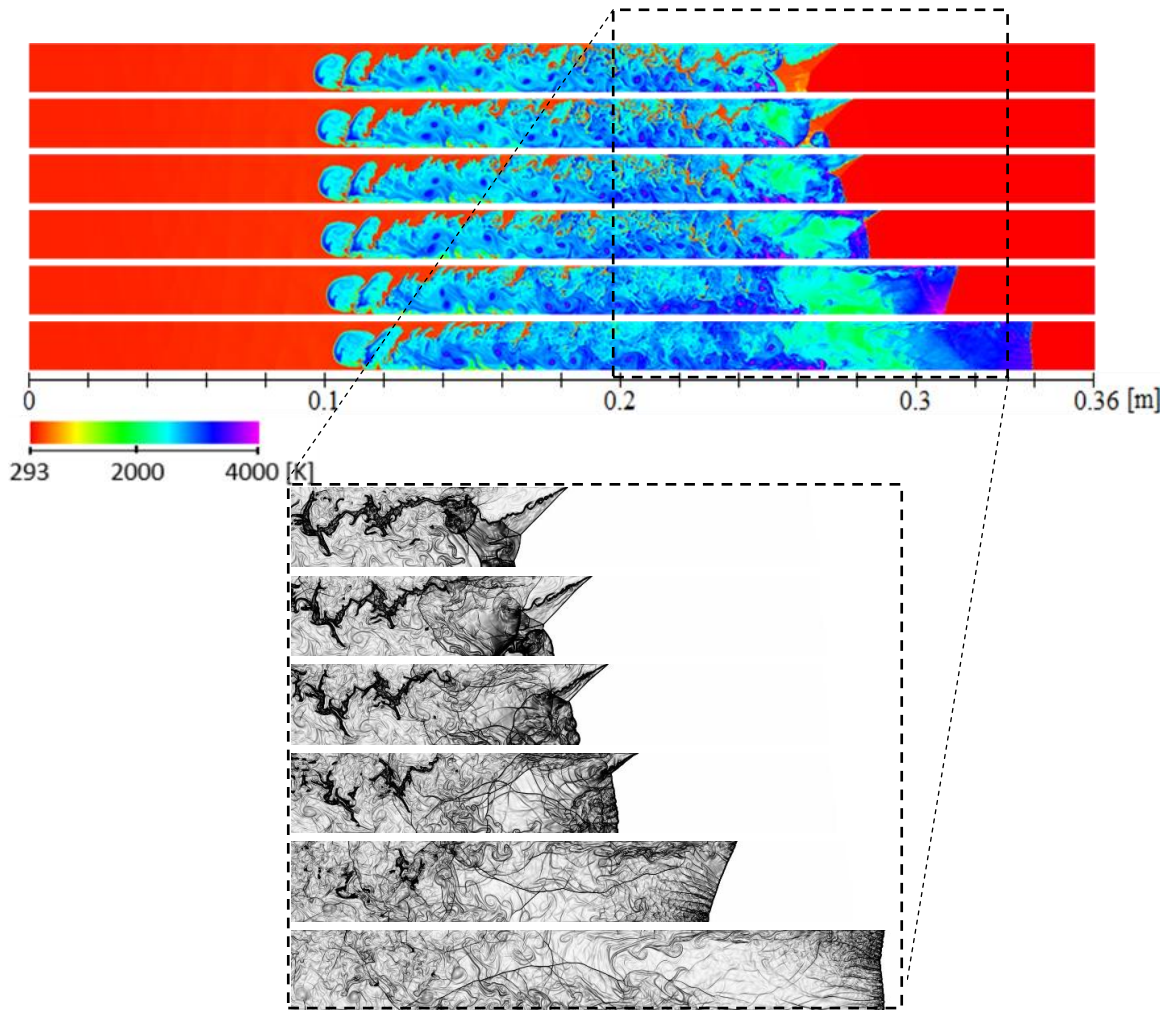


FIGURE 4. Temperature fields and zoom-in schlieren plots showing the onset of detonation

The interaction by the shock causes the flame surface to increase, leading to an increase in the rate of energy release. Besides the burn-out rate of flame folds, flame acceleration is further supported by the increased presence of small-scale turbulence which can be seen in the last panel of Fig. 3. In addition, the effect of the boundary layer becomes also significant and shocked reactants begin to react near the top wall boundary which can be seen in Fig. 4. Between the flame kernels and the top boundary a large amount of shocked reactant exists, however it gradually reduces in size due to the elongation of the flame brush in the y -direction and the ignition of combustible near the wall boundary.

The flow ahead of the flame brush is also affected by compression waves that have been generated by the interaction and reflection processes and propagate downstream. These waves pre-condition the temperature of the reactants, leading to an increased reaction rate. The compression waves ahead of the flame brush also affect the flame kernels, and as a result they convect and slightly deform, becoming less circular on their left side. It should also be noted that, until the flame kernels interact with the incident shock, they continue to burn outwards due to heat and mass diffusion, thus, increase in size. In the temperature fields of both Figs. 3 and 4, the turbulent flame brush development after multiple interactions is shown more clearly.

Through the interaction with subsequent discrete flames, the leading shock strength continues to increase and also a wrinkled, turbulent flame brush is formed from the merging of multiple flame surfaces. A series of compression waves is emitted from the shock-flame interactions and reflected from the upper solid wall resulting in a higher, shock-induced, temperature of the surrounding reactants. These intense fluctuations create small variations in the temperature ahead of the flame brush and act to increase the overall rate of energy release in the system. Multiple shock-flame interactions eventually develop a hot spot (or localized explosion) and trigger transition to detonation as evidenced by the appearance of a frontal cellular structure [11, 44-46] as shown in Fig. 4.

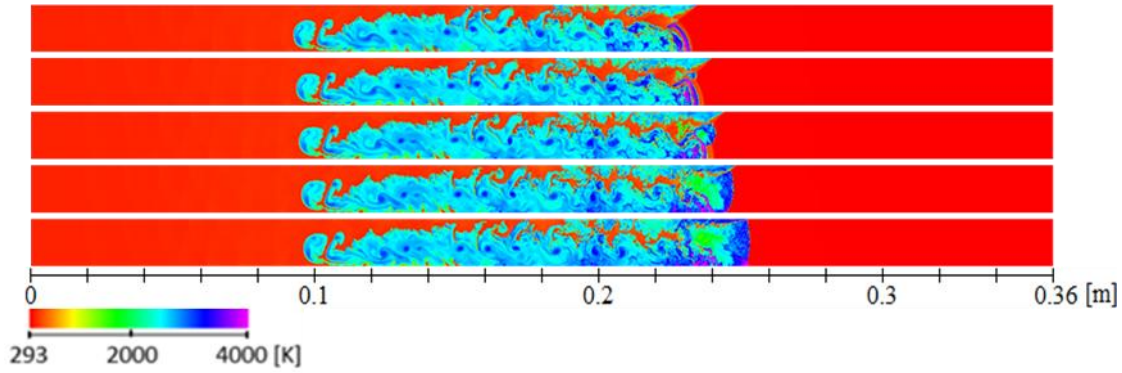


FIGURE 5. Temperature plots, onset of detonation for Navier-Stokes simulation with double resolution the original grid resolution using the finest grid of $\Delta x = 23.5 \mu\text{m}$

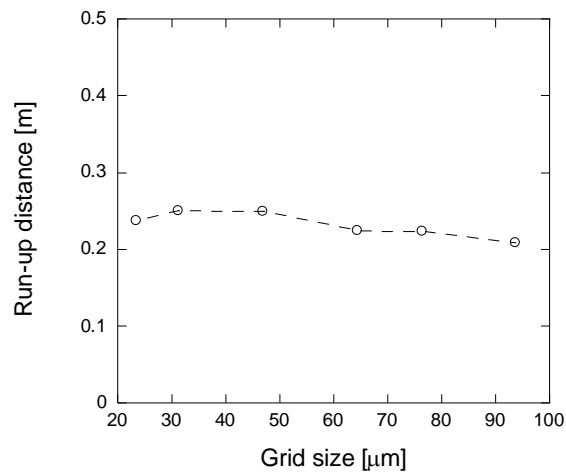


FIGURE 6. DDT run-up distances obtained using numerical grid resolution for the default settings

3.2 Effects of numerical grid resolution

The present results show that the resulting DDT process involves a complex turbulence flame brush formation via a series of shock-flame and boundary layer interactions. In order to verify that any further grid refinement does not significantly affect the results, one more simulation was performed with increased grid resolution. An additional AMR level was thus added, leading to a grid resolution of $\Delta x = 23.5 \mu\text{m}$ at the highest level. The results can be seen in the temperature plots of Fig. 5. Overall, the flow development is similar to the original resolution simulation. In both cases, the onset of detonation occurs in unreacted material that is confined between turbulent flame brushes. Nevertheless, due to the higher resolution, finer details of the turbulent

flow can be seen, and the flame brush surface appears to be slightly more wrinkled compared to that resulting from the simulations with the default grid resolution. The additional small wrinkles indicate an increased flame surface, which leads to a higher burning rate, and thus a faster acceleration of the flame brush. This explains the slightly earlier position of the explosion bubble in this higher-resolution simulation. Therefore, as demonstrated, the default grid resolution of $\Delta x = 47 \mu\text{m}$ is sufficient for the simulation of the phenomenon. As discussed in the subsequent section, the characteristic parameter we are interested is the DDT run-up distance and onset time. These are defined as the location and time at which an explosion occurs and an abrupt increase in pressure above the detonation level is detected anywhere within the computational flow field. This resolution test ensures convergence of the DDT run-up distance using the default resolution, see Fig. 6. The difference incurred by increasing the grid resolution is less than 10%. One interesting observation in Fig. 6 is that a relatively shorter DDT distance is resulted from the simulation with further coarser grid resolution. Although finer features of the turbulence cannot be resolved, the numerical diffusion due to the low grid resolutions does help to promote the transition from deflagration to detonation.

3.3 Effects of dissipative transport

To demonstrate the importance of transport effects, a simulation with the effects of viscosity, thermal conduction, and molecular diffusion removed from the governing equations is performed to determine their impact on DDT (referred to as Euler simulation). The results of the simulation can be seen in Fig. 7. Multiple wave reflections between the bottom boundary and the flame brush surface lead to the conditioning of the fuel-air mixture and the onset occurs at the reflective boundary. The full transition to a detonation wave does not occur inside the current domain boundaries. However, based on the explosion feature that occurs at the symmetry

boundary near the end of the domain, a detonation wave will likely form outside the domain boundaries. Compared to the simulation with Navier-Stokes equations, the onset of detonation occurs further downstream and at a significantly later time. These results therefore indicate that the suppression of turbulence and burning rate strongly affects the DDT phenomenon. The fact that the Euler simulation does not undergo transition at the same time or location as in the Navier-Stokes case demonstrates the sensitivity of this process to the method of simulation.

Two-dimensional numerical simulations have been obtained to observe the propagation of a weak incident shock wave into multiple cylindrical flames and its subsequent amplification via intense wave interactions and reflections. The simulation results demonstrate that DDT is possible via a series of shock-flame interactions. In the Navier-Stokes simulation, the onset of detonation is observed from the development of a hot spot ahead of the flame brush. It forms through an increase in the rate of energy release caused by the increase of flame surface area, and greater shock temperatures from amplifying shock near the top wall through pressure wave reflection and coalescence. In the absence of physical diffusion and viscosity where turbulence and the burning of the turbulent flame brush are suppressed, the Euler simulation also shows that the intense flow fluctuations generated by the interactions of shocks, boundary, and flames can still create the conditions under which deflagration-to-detonation transition can be realized.

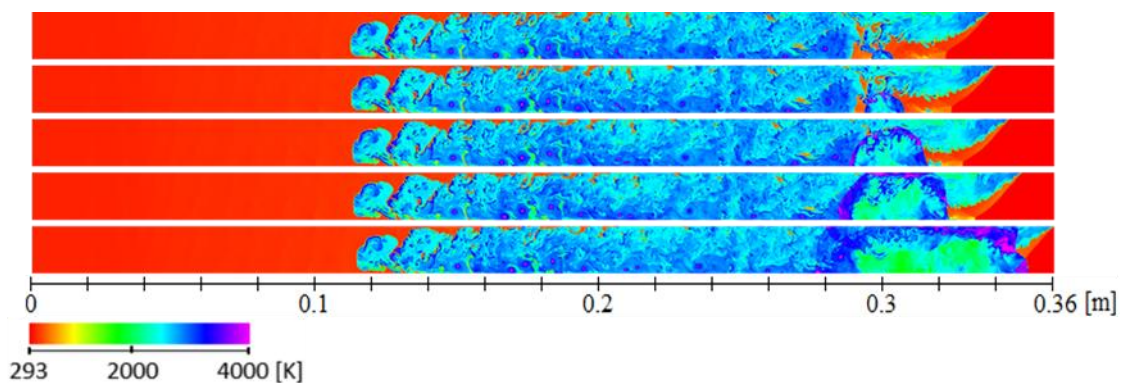


FIGURE 7. Temperature plots, onset of detonation for Euler simulation

3.4 A parametric study

DDT in a smooth tube is a stochastic and sensitive phenomenon which can vary significantly even under a small parameter change, leading to different characteristics (run-up distance and onset time), whereas the transition might not even occur inside the domain boundaries, as was demonstrated previously for the simulation with the Euler equations. For that reason, a series of Navier-Stokes simulations were performed in which certain parameters were modified to determine their impact on DDT and identify the changes that could lead to a reduction of the run-up distance and time of detonation onset. It is worth noting that because of the stochastic nature of the DDT process, it creates an unavoidable uncertainty in the assessment on the effects of each varying parameter and some fluctuating behaviors of data are thus expected. The simulation results can thus be discussed at best on their overall trends.

3.4.1. Effects of scale

The first simulation parameter under consideration was the channel height L_y . The values that were considered were between 9.75 mm and 16.5 mm, since that was the highest value for which DDT would occur inside the domain and was not affected by the domain resolution, as was demonstrated in the resolution test. For this parametric study, the radius of the cylindrical flame kernels was set to 5 mm. The choice of reducing the channel height was made in order to enhance the effect of shock-boundary layer interaction in the transition process and was indicated by the increased size of the induction zone near top boundary as compared to the previous default simulation. The results of the simulations are summarized in Fig. 8.

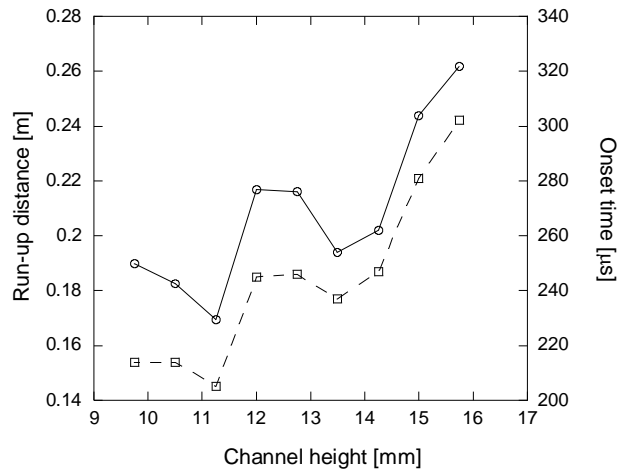


FIGURE 8. The effect of channel height on the DDT run-up distance (solid line) and onset time (dashed line)

As seen in Fig. 8, the channel height plays a prominent role in flame acceleration or DDT [47]. In the present simulation study, reducing the channel height from the initial value of 16.5 mm, while keeping all other lengths constant leads to the reduction of characteristic values of DDT, up to a minimum for the simulation with 11.25 mm channel height. For the case of $L_y = 11.25$ mm, the run-up distance is equal to 0.17 m and the onset time of 205 μs . Further reduction of the channel height has an adverse effect of causing a noticeable increase of run-up distance, whereas onset time varies only slightly.

Figure 9 shows the temperature plots at the onset of detonation for three simulations with 11.25 mm, 13.5 mm and 15.75 mm channel heights. For the simulation with the minimum run-up distance, the onset of detonation occurs above the 10th flame kernel, where a local explosion is induced near the top solid boundary due to the various mechanisms explained previously. The lower run-up distance observed is a result of the increased contribution of the shock-boundary interaction in the transition process as well as the proper synchronization of the chemical energy release with the shock wave. Reducing the channel height also promotes compression wave reflections and the role of turbulence induced by the boundary layer becomes more significant.

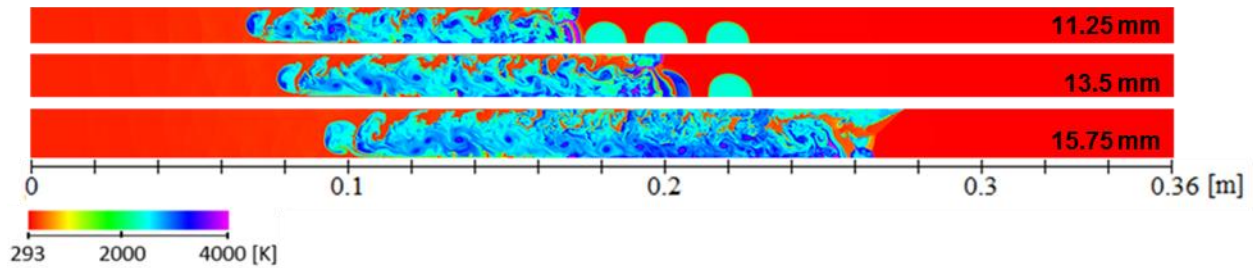


FIGURE 9. Temperature plots at the onset of detonation for 11.25 mm, 13.5 mm and 15.75 mm domain height

The second parameter under consideration was the amplitude of the flame kernels (i.e., the initial radius of the cylindrical flames). Practically, this parameter can be controlled by different spark ignition times in real experiment. For this series of simulations, the domain height was equal to $L_y = 15$ mm, five levels of AMR were used with the same resolution at the top level as previously. The amplitude values considered were between 4.4 mm and 6.6 mm. The results from these simulations are given in Fig. 10 and Fig. 11.

Increasing flame amplitude has generally a positive impact on DDT. Larger flame amplitude implies larger flame surface; the R-M instabilities from the shock-flame interaction will also become severe as the flame amplitude increases. As the amplitude is increased, the values of DDT distance and time start to gradually decrease, a minimum run-up distance is achieved with the flame amplitude has changed to 6.2 mm. The trend is similarly to the channel height variation, suggesting that a key parameter facilitating DDT is the ratio between the channel height and the ignited kernel size. Nevertheless, if the initial flame kernel size is approaching further to the channel height, not enough unburned reactant and energy release may exist to couple and amplify any shock or turbulence promoting the onset of DDT.

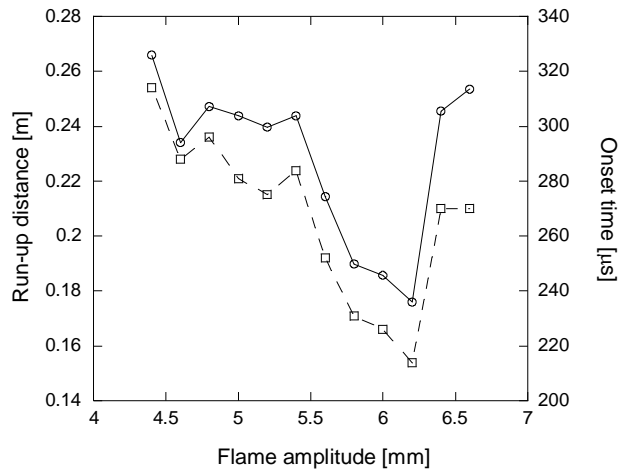


FIGURE 10. The effect of laminar flame amplitude on the DDT run-up distance (solid line) and onset time (dashed line)

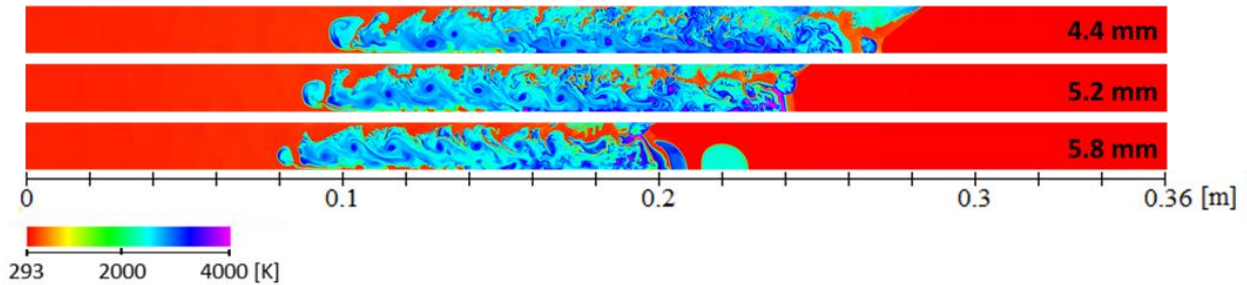


FIGURE 11. Temperature plots at the onset of detonation for 4.4 mm, 5.2 mm and 5.8 mm flame amplitude

In the next series of simulations the distance between flame kernels was varied for a domain channel height equal to $L_y = 15$ mm, five AMR levels and the same resolution $\Delta x = 47$ μ m again at the highest level. Results showing the effect of distance between flame kernels are given in Fig. 12 and Fig. 13. Similar to the flame amplitude, practical flame kernel spacing is achieved by using different spark distance and properly controlling the spark timing to generate each flame kernel. Qualitatively, it controls the coherence between the gas dynamics and energy release. When the flame kernels are separated too far away, the potential gain from each shock-flame kernel collision causing an increased rate of energy release and turbulence may not be coupled to generate the proper condition for DDT. If the distance is too close, similar to the effect of

reducing significantly the channel height or increasing the flame kernel amplitude, not enough unburned reactant is present to cohere the energy release with the flow, (i.e., approaching to a normal shock interacting with a long flat flame kernel). Hence the chemical energy release is insufficient to coherently amplify the strength of the shock front (as it runs away from the flame brush shown in Fig. 13) or generate a high speed turbulent flame brush.

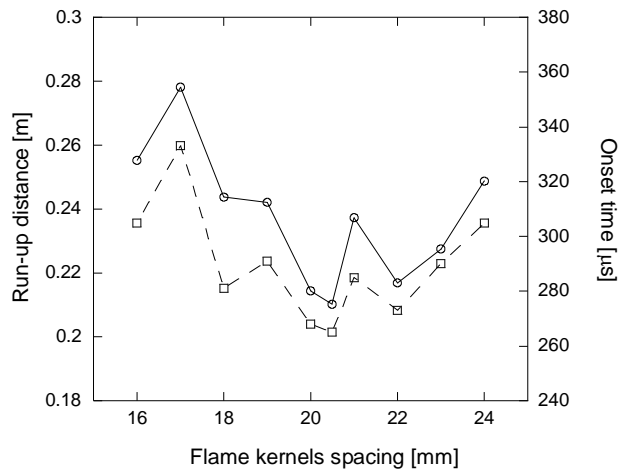


FIGURE 12. The effect of distance between flame kernels on the DDT run-up distance (solid line) and onset time (dashed line).

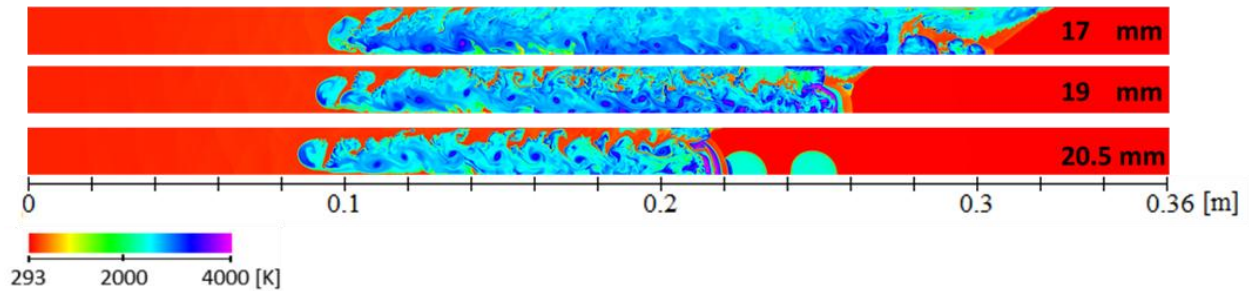


FIGURE 13. Temperature plots at the onset of detonation for 17 mm, 19 mm and 20.5 mm flame kernel distance

As previously mentioned, the flame surface has been modeled as a contact discontinuity between the unburned cold reactants and hot combustion products. Having a discontinuity instead of a diffusive interface could potentially affect the DDT phenomenon. For that reason, a complementary series of simulations were also performed by placing the incident shock wave further upstream, while maintaining all other parameters, in order to allow the flame kernel

surface to diffuse in the additional time until the first shock-flame interaction occurs. The shock placements considered were at 1 mm and 3 mm distance from the left boundary and the results were compared to the original 6 mm placement.

As shown in Fig. 14, the initial shock wave location has no significant effect on the DDT run-up distance which remains essentially constant. A small onset time difference can be attributed to the additional required time until the shock begins interacting with the first flame kernel. Therefore, modeling the flame surface as a contact discontinuity compared to a diffusive flame surface does not affect the phenomenon.

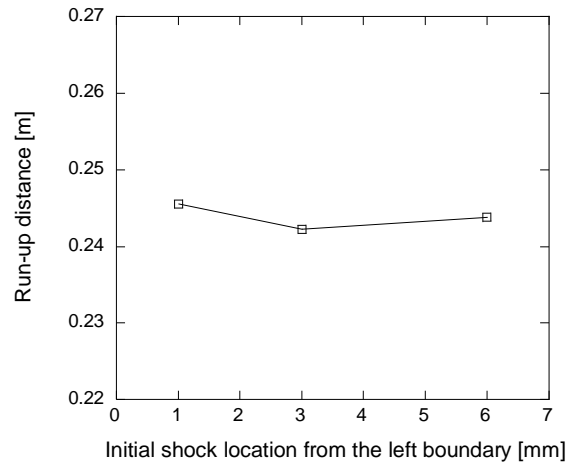


FIGURE 14. Run-up distance dependence on the initial incident shock wave position

3.4.2. Effects of incident shock parameters

Up till now the parametric study focuses primarily on the effect of different length scales on the DDT via multiple shock-flame interactions. The last sets of simulations considered the strength of the incident shock and the number of initial laminar flame kernels. First, the incident shock strength was reduced to a value of $M_o = 1.6$, while maintaining all other length scale parameters fixed, i.e., flame spacing $l = 18$ mm, flame amplitude $r = 5$ mm and channel height of $L_y = 16.5$ mm. The simulations also showed that a weaker incident shock can still induce DDT, see Fig. 15.

In addition, the flow field inside the flame brush formed from the shock interaction and coalescence of individual flames is relatively less turbulent. The onset of detonation is again seen from a localized explosion created in the flow by various wave interactions ahead of the flame. For the smaller M_o , the hot spot is formed closer to the top wall instead. The onset of detonation occurs at a much later time $t \sim 306$ s but yet the run-up distance for the detonation onset is close to the condition with $M_o = 1.80$. However, the dependence of DDT run-up distance is not totally clear and requires a further examination as follows shortly. From the present results, it is found that the DDT occurs at random locations, where an appropriate condition is produced through a series of shock-flame interactions for the coupling between the heat release and gas dynamics.

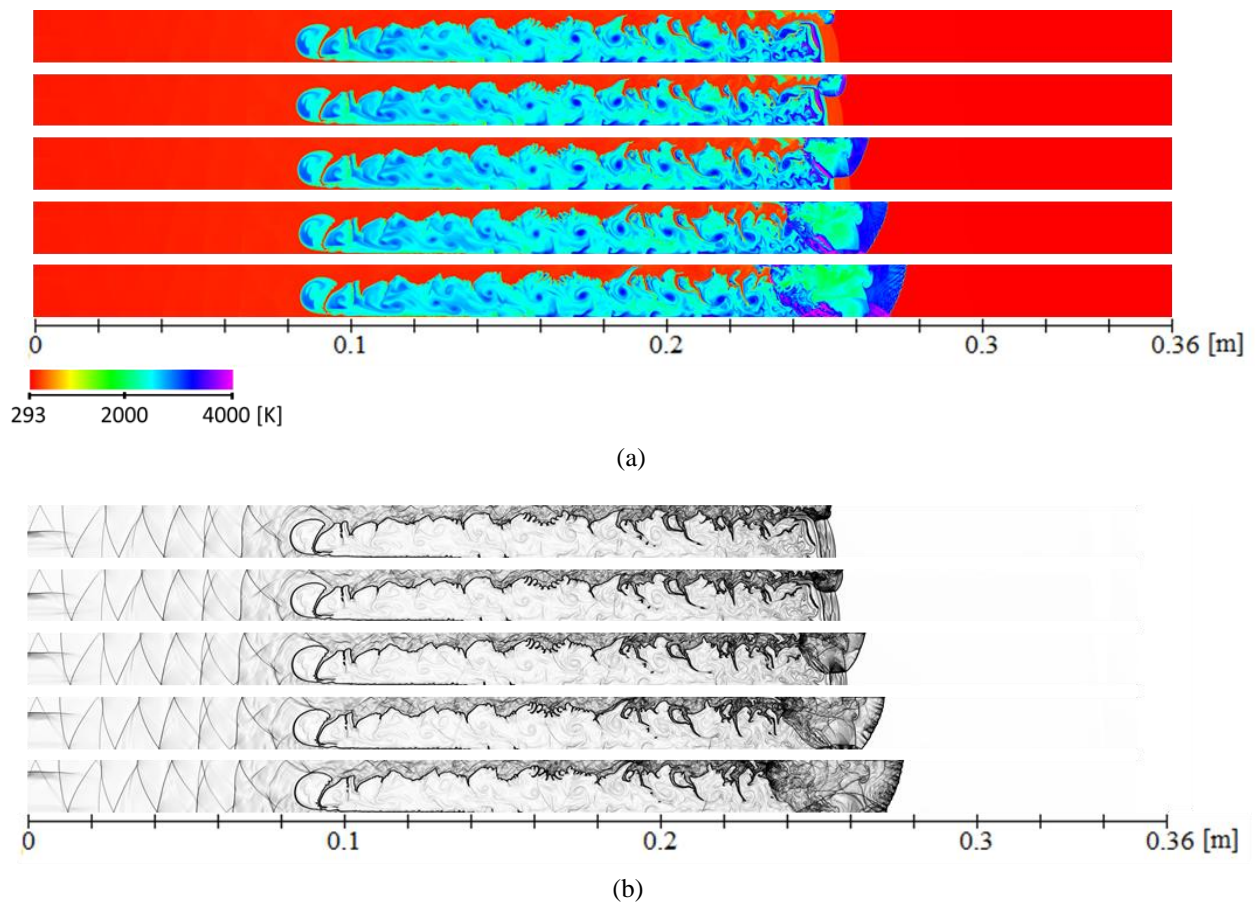


FIGURE 15. a) Temperature contours and b) Schlieren plots at later stage of the evolution for $M_o = 1.60$ showing the detonation initiation from a localized explosion near the top solid wall

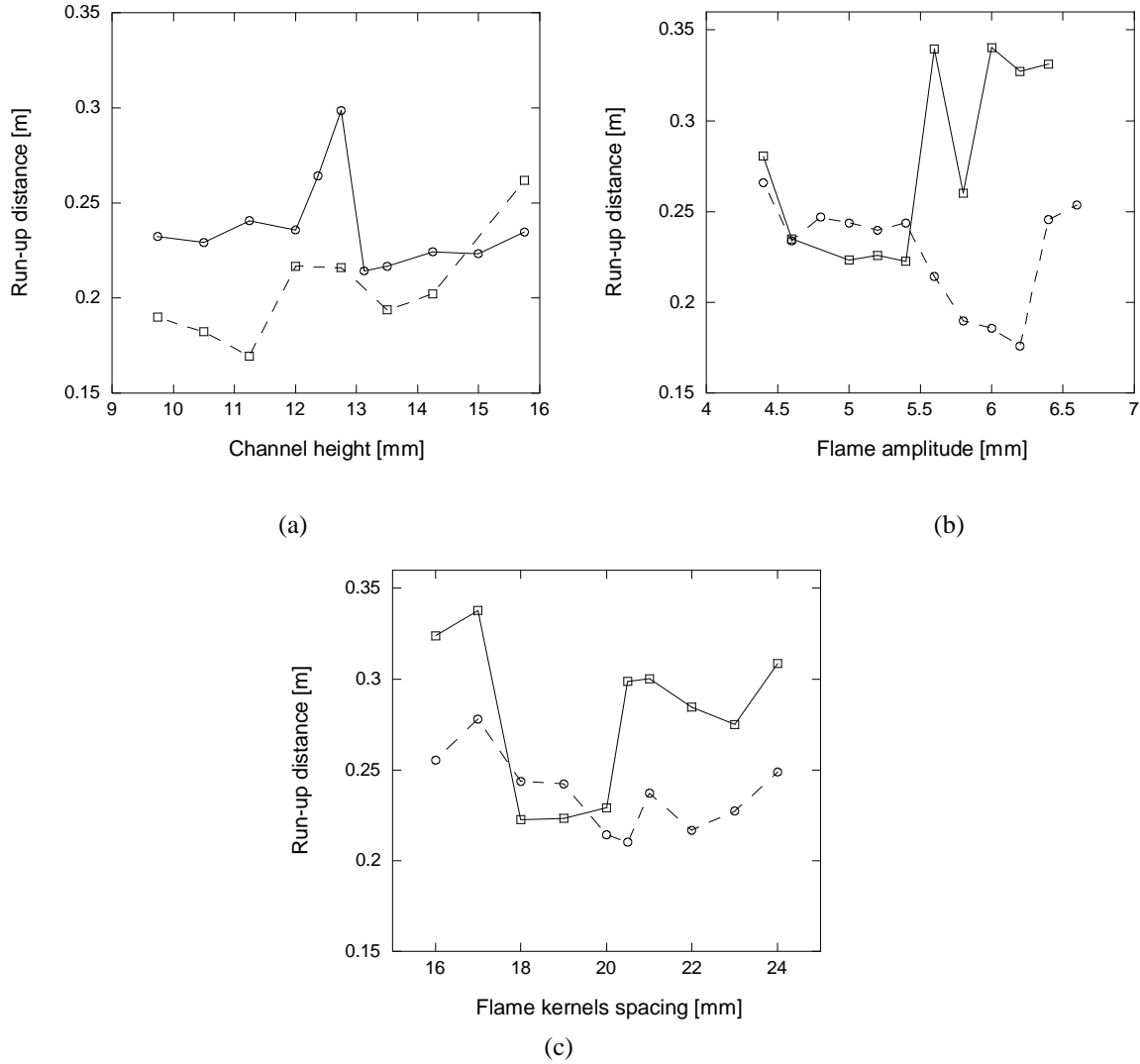


FIGURE 16. Run-up distance dependence on a) Channel height; b) flame amplitude; and c) flame kernels spacing for incident shock strength $M_0 = 1.6$ (solid line) and $M_0 = 1.8$ (dashed line).

The effects of incident shock Mach number on DDT run-up distance are again investigated through a parametric study of varying the channel height, flame spacing and the flame amplitude for incident shock strength $M_0 = 1.6$, and the results were compared to the ones for the original $M_0 = 1.8$ shock strength. These results are summarized in Figs. 16.

Referring to these figures, the simulations with $M_0 = 1.6$ demonstrate similar dependence on the flame kernel spacing, however at lower shock Mach number they appear to be more

sensitive, with larger stochastic variations of characteristics and overall longer DDT run-up distance. For the dependence on flame spacing and amplitude, the difference between these results can be attributed mainly to the increase in temperature of the shocked reactant (and hence, energy release rate) with increasing the M_o . Reducing M_o causes a reduction in the energy release rate with lower post-shock temperature and hence, a closer flame spacing is needed for synchronizing the chemical energy release with the gas dynamics. It also requires a larger volume of unburned mixture to release sufficient energy to facilitate the shock amplification and flame acceleration, which explains the trend of longer DDT run-distance at smaller domain height and larger flame amplitude as compared to the results of $M_o = 1.80$. Additionally, reducing the M_o weakens the interaction of the leading shock with the boundary layer, contributing the overall global effect of increasing the distance required for DDT.

3.4.3. Effects of flame kernels number

Finally, the simulations with domain height, flame amplitude and spacing variations were performed to look at the effect of a reduced flame kernel number. Results obtained for 10 and 12 flame kernels with $M_o = 1.80$ are given in Fig. 17. As can be seen in the figure, almost all 12 kernel simulations demonstrate equal or slightly lower run-up distance and time compared to the 10 kernels simulations. For lower flame kernel numbers, DDT sometimes may not even occur within the initial flame kernel array, as illustrated in Fig. 18 for the case with 16.5 mm channel height. It appears that increasing the number of ignited flame kernels may facilitate and ensure DDT will occur within the controlled flame array region.

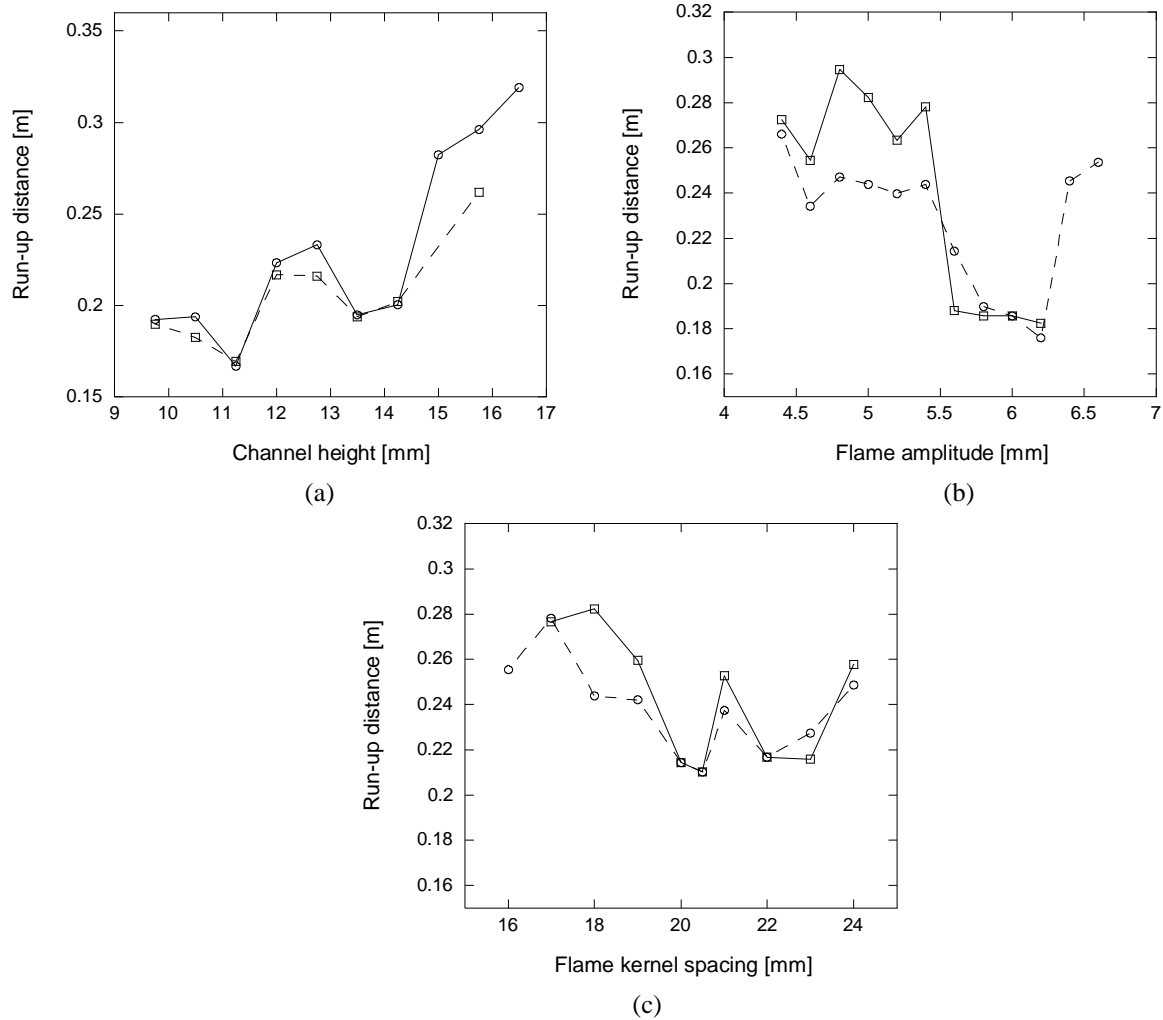


FIGURE 17. Run-up distance dependence on a) Channel height; b) flame amplitude; and c) flame kernels spacing for 10 (solid line) and 12 (dashed) flame kernels

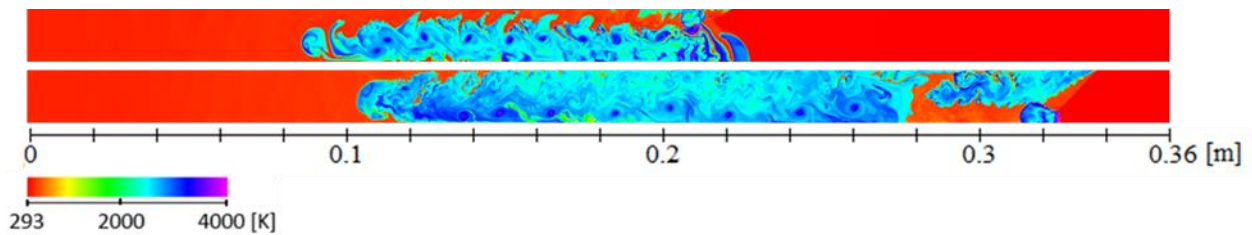


FIGURE 18. Temperature plots at onset of detonation for 12 flame kernels (top) and 10 flame kernels (bottom)

In order to assess the influence of various physical parameters on the transition event and to explore any scaling relationship among them, the above parametric study performs a range of simulations considering the effects of domain size, ignited flame arrangements and initial

conditions. Practically in real experiments, these parameters can be varied physically by controlling the ignition time and distance between each spark. The present study demonstrates that these aforementioned parameters can significantly control DDT and it is possible to optimize these parameters to achieve DDT at a short run-up distance to obtain a self-propagating detonation. Nevertheless, due to the stochastic nature of the reactive system, the exact quantitative relationship between the DDT characteristics with these physical parameters cannot be fully established and further quantitative investigation is desirable.

4. CONCLUSION

In this investigation, two-dimensional numerical simulations were performed for a planar shock wave interacting with multiple flame kernels. The results of the simulations demonstrate that these interactions amplify the leading shock wave and accelerate the flame brush, resulting in a deflagration-to-detonation transition (DDT). As seen in the simulations, a DDT is divided into four phases: The generation of R-M instability increasing turbulence and energy release rate, the acceleration of the flame brush, the formation of an explosion bubble, and the final formation of detonation wave. For the Navier-Stokes simulations, the acceleration of the flame brush is promoted by the intense turbulence generated through shock-flame and shock-boundary interactions. The explosion center develops ahead of the flame brush in the unreacted shocked material as a result of pressure wave reflections and coalescence and higher post-shock temperatures near the top boundary. In the Euler simulations, although the flame acceleration and the formation of hot spot are affected by the suppression of turbulence and burning rate, DDT can still be achieved by the flow fluctuations generated through shock-flame interactions and wave reflections from boundary. The explosion center for these simulations occurs later and further downstream compared to the Navier-Stokes simulations.

Finally, through a series of numerical simulations it was demonstrated that DDT is significantly affected when certain key parameters are modified. The parameters considered were the domain height, flame amplitude, flame spacing, number of flame kernels and incident shock speed. Modifying these parameters affects the acceleration process and the formation of hot spots, potentially resulting in a reduced run-up distance and time of detonation onset for certain parameter values. The simulations with reduced incident shock strength also show that a strong incident shock is not always favored for DDT, but a proper synchronization of the chemical energy release rate with the gas dynamics is more important by appropriately tuning flame configuration and boundary size.

While using the one-step ideal reaction model, the coupling between the heat release and flow dynamics from the shock- laminar flame kernels interaction leading to the onset of DDT can be elucidated. However, the more quantitative effect of chemistry such as the importance of reactive radicals generation cannot be revealed. In future efforts, computational study using detailed chemistry are thus needed for more quantitative simulations, i.e., to further pinpoint the critical conditions and compare with experimental data. High-order numerical schemes will also be beneficial to better capture the mixing and dynamics within the resulting turbulence flows from the shock-multiple flame kernels interaction.

ACKNOWLEDGMENTS

This work is supported by the Natural Sciences and Engineering Research Council of Canada NSERC (No. RGPIN-2017-06698).

REFERENCES

1. K. Kailasanath, Recent developments in the research on pulse detonation engines, *AIAA J.* **41** (2003) 145-159. <https://doi.org/10.2514/2.1933>
2. P. Wolanski, Detonative propulsion, *Proc. Combust. Inst.* **34** (2013) 125-158. <https://doi.org/10.1016/j.proci.2012.10.005>
3. T. Wang, Y. Zhang, H.H. Teng, Z.L. Jiang, H.D. Ng, Numerical study of oblique detonation wave initiation in a stoichiometric hydrogen-air mixture, *Phys. Fluids* **27** (2015) 096101. <https://doi.org/10.1063/1.4930986>
4. Y. Liu, W. Zhou, Y. Yang, Z. Liu, J. Wang, Numerical study on the instabilities in H₂-air rotating detonation engines, *Phys. Fluids* **30** (2018) 046106. <https://doi.org/10.1063/1.5024867>
5. C. Li, K. Kailasanath, E. S. Oran, Detonation structures behind oblique shocks, *Phys. Fluids* **6** (1994) 1600–1611. <https://doi.org/10.1063/1.868273>
6. J.H.S. Lee, A.J. Higgins, Comments on criteria for direct initiation of detonation, *Philos. Trans. R. Soc. A* **357** (1999) 3503-3521. <https://doi.org/10.1098/rsta.1999.0506>
7. J.H.S. Lee, Initiation of gaseous detonation, *Ann. Rev. Phys. Chem.* **28** (1977) 75-104. <https://doi.org/10.1146/annurev.pc.28.100177.000451>
8. G. Ciccarelli, S. Dorofeev, Flame acceleration and transition to detonation in ducts, *Prog. Combust. Sci.* **34** (4) (2008) 499-550. <https://doi.org/10.1016/j.pecs.2007.11.002>
9. G.D. Roy, S.M. Frolov, A.A. Borisov, D.W. Netzer, Pulse detonation propulsion: challenges, current status, and future perspective, *Prog. Energy Combust. Sci.* **30** (2004) 545-672. <https://doi.org/10.1016/j.pecs.2004.05.001>
10. E.S. Oran, V.N. Gamezo, Origins of the deflagration-to-detonation transition in gas-phase combustion, *Combust. Flame* **148** (1-2) (2007) 4-47. <https://doi.org/10.1016/j.combustflame.2006.07.010>
11. J.H.S. Lee, *The Detonation Phenomenon*, Cambridge University Press, New York, 2008.
12. E. Schultz, E. Wintenberger, J.E. Shepherd, Investigation of deflagration to detonation transition for application to pulse detonation engine ignition systems, in: *Proceedings of the 16th JANNAF Propulsion Symposium*. Chemical Propulsion Information Agency, 1999.

13. E.S. Oran, Understanding explosions – From catastrophic accidents to the creation of the Universe, *Proc. Combust. Inst.* **35** (1) (2015) 1-35. <https://doi.org/10.1016/j.proci.2014.08.019>
14. A.M. Khokhlov, E.S. Oran, G.O. Thomas, Numerical simulation of deflagration-to-detonation transition: the role of shock–flame interactions in turbulent flames, *Combust. Flame* **117** (1-2) (1999) 323-339. [https://doi.org/10.1016/S0010-2180\(98\)00076-5](https://doi.org/10.1016/S0010-2180(98)00076-5)
15. A.M. Khokhlov, E.S. Oran, Numerical simulation of detonation initiation in a flame brush: The role of hot spots, *Combust. Flame* **119** (1999) 400-416. [https://doi.org/10.1016/S0010-2180\(99\)00058-9](https://doi.org/10.1016/S0010-2180(99)00058-9)
16. V.N. Gamezo, A.M. Khokhlov, E.S. Oran, The Influence of shock bifurcations on shock-flame interactions and DDT, *Combust. Flame* **126** (2001) 1810-1826. [https://doi.org/10.1016/S0010-2180\(01\)00291-7](https://doi.org/10.1016/S0010-2180(01)00291-7)
17. S.M. Frolov, Initiation of strong reactive shocks and detonation by traveling ignition pulses, *J. Loss Prev. Proc. Ind.* **19** (2006) 238-244. <https://doi.org/10.1016/j.jlp.2005.04.006>
18. Ya. B. Zel'dovich, V.B. Librovich, G.M. Makhviladze, G.I. Sivashinsky, On the development of detonation in a non-uniformly preheated gas, *Acta Astro.* **15** (1970) 313-321.
19. A.M. Bartenev, B.E. Gelfand, Spontaneous initiation of detonations, *Prog. Energy Comb. Sci.* **26** (1) (2000) 29-55. [https://doi.org/10.1016/S0360-1285\(99\)00007-6](https://doi.org/10.1016/S0360-1285(99)00007-6)
20. J.H.S. Lee, I.O. Moen, The mechanism of transition from deflagration to detonation in vapour cloud explosions, *Proc. Energy Comb. Sci.* **6** (1979) 359-389. [https://doi.org/10.1016/0360-1285\(80\)90011-8](https://doi.org/10.1016/0360-1285(80)90011-8)
21. A.M. Khokhlov, E.S. Oran, J.C. Wheeler, A theory of deflagration-to-detonation transition in unconfined flames, *Combust. Flame* **108** (1997) 503-517. [https://doi.org/10.1016/S0010-2180\(96\)00105-8](https://doi.org/10.1016/S0010-2180(96)00105-8)
22. A.K. Kapila, D.W. Schwendeman, J.J. Quirk, T. Hawa, Mechanisms of detonation formation due to a temperature gradient, *Combust. Theory Modell.* **6** (2002) 553-594. <https://doi.org/10.1088/1364-7830/6/4/302>
23. Ya. B. Zel'dovich, A.S. Kompaneets, *Theory of Detonation*, Gostekhteorizdat, Moscow, 1955.

24. S.M. Frolov, V. Ya. Basevich, V.S. Aksenov, S.A. Polikhov, Detonation initiation by controlled triggering of electric discharges, *J. Prop. Power* **19** (4) (2003) 573-580. <https://doi.org/10.2514/2.6168>
25. Z.M. Hu, H.S. Dou, B.C. Khoo, Rapid detonation initiation by sparks in a short duct: a numerical study, *Shock Waves* **20** (2010) 241-249. <http://doi.org/10.1007/s00193-010-0252-4>
26. K.R. Bates, N. Nikiforakis, D. Holder, Richtmyer-Meshkov instability induced by the interaction of a shock wave with a rectangular block of SF₆, *Phys. Fluids* **19** (3) (2007) 036101. <https://doi.org/10.1063/1.2565486>
27. K.R. Bates, *Numerical Simulation and Analysis of the Transition to Detonation in Gases*, PhD Thesis, University of Cambridge, UK, 2005.
28. D.A. Kessler, V.N. Gamezo, E.S. Oran, Simulations of flame acceleration and deflagration-to-detonation transitions in methane-air systems, *Combust. Flame* **157** (2010) 2063-2077. <https://doi.org/10.1016/j.combustflame.2010.04.011>
29. T. Ogawa, E.S. Oran, V.N. Gamezo, Numerical study on flame acceleration and DDT in an inclined array of cylinders using an AMR technique, *Computer Fluids* **85** (1) (2013) 63-70. <https://doi.org/10.1016/j.compfluid.2012.09.029>
30. T. Ogawa, V.N. Gamezo, ES Oran, Flame acceleration and transition to detonation in an array of square obstacles, *J. Loss Prev. Proc. Indust.* **26** (2) (2013) 355-362. <https://doi.org/10.1016/j.jlp.2011.12.009>
31. G.B. Goodwin, E.S. Oran, Premixed flame stability and transition to detonation in a supersonic combustor, *Combust. Flame* **197** (2018) 145-160. <https://doi.org/10.1016/j.combustflame.2018.07.008>
32. G.B. Goodwin, R.W. Houim, E.S. Oran, Shock transition to detonation in channels with obstacles, *Proc. Combust. Inst.* **36** (2) (2017) 2717-2724. <https://doi.org/10.1016/j.proci.2016.06.160>
33. E.F. Toro, *Riemann Solvers and Numerical Methods for Fluid Dynamics*, 3rd ed., Springer, Berlin, 2006.
34. M.J. Berger, J. Olinger, Adaptive mesh refinement for hyperbolic partial differential equations, *J. Comput. Phys.* **53** (1984) 484-512. [https://doi.org/10.1016/0021-9991\(84\)90073-1](https://doi.org/10.1016/0021-9991(84)90073-1)

35. S.D. Hern, *Numerical Relativity and Inhomogeneous Cosmologies*, PhD Thesis, University of Cambridge, UK, 1999.
36. H.D. Ng, A.J. Higgins, C.B. Kiyanda, M.I. Radulescu, J.H.S. Lee, K.R. Bates, N. Nikiforakis, Nonlinear dynamics and chaos analysis of one-dimensional pulsating detonations, *Combust. Theor. Modell.* **9** (2005) 159–170. <https://doi.org/10.1080/13647830500098357>
37. G. Cael, H.D. Ng, K.R. Bates, N. Nikiforakis, M. Short, Numerical simulation of detonation structures using a thermodynamically consistent and fully conservative (TCFC) reactive flow model for multi-component computations, *Proc. R. Soc. London A*, **465** (2009) 2135-2153. <https://doi.org/10.1098/rspa.2008.0371>
38. G.H. Markstein, Flow disturbances induced near a slightly wavy contact surface, or flame front, traversed by a shock wave, *J. Aero. Sci.* **24** (1957) 238– 39.
39. G.H. Markstein, A shock-tube study of flame front-pressure wave interaction, *Proc. Combust. Inst.* **6** (1) (1957) 387-398. [https://doi.org/10.1016/S0082-0784\(57\)80054-X](https://doi.org/10.1016/S0082-0784(57)80054-X)
40. M. Brouillette, The Richtmyer-Meshkov instability, *Annu. Rev. Fluid Mech.* **34** (2002) 445-468. <https://doi.org/10.1146/annurev.fluid.34.090101.162238>
41. L. Massa, P. Jha, Linear analysis of the Richtmyer-Meshkov instability in shock-flame interactions, *Phys. Fluids* **24** (2012) 056101. <https://doi.org/10.1063/1.4719153>
42. D. Ranjan, J. Oakley, R. Bonazza, Shock-bubble interactions, *Annu. Rev. Fluid Mech.* **43** (2011) 117-140. <https://doi.org/10.1146/annurev-fluid-122109-160744>
43. J. Glimm, M.J. Graham, J. Grove, X.L. Li, T.M. Smith, D. Tan, F. Tangerman, Q. Zhang, Front tracking in two and three dimension, *Comput. Math. Appl.* **35** (1998) 1-11. [https://doi.org/10.1016/S0898-1221\(98\)00028-5](https://doi.org/10.1016/S0898-1221(98)00028-5)
44. M.V. Papalexandris, A. Leonard, P.E. Dimotakis, Unsplit algorithms for multidimensional systems of hyperbolic conservation laws with source terms, *Comput. Math. Appl.* **44** (1-2) (2002) 25-49. [https://doi.org/10.1016/S0898-1221\(02\)00128-1](https://doi.org/10.1016/S0898-1221(02)00128-1)
45. W. Han, Y. Gao, C. Wang, C.K. Law, Coupled pulsating and cellular structure in the propagation of globally planar detonations in free space, *Phys. Fluids* **27** (2015) 106101. <https://doi.org/10.1063/1.4933134>

46. H.D. Ng, F. Zhang, Detonation instability, in: Zhang, F. (ed.) *Shock Wave Science and Technology Library, Detonation Dynamics*, Vol. 6, Chap. 3. Springer, Berlin, 2012. <https://doi.org/10.1007/978-3-642-22967-1>
47. W. Han, Y. Gao, C.K. Law, Flame acceleration and deflagration-to-detonation transition in micro- and macro-channels: An integrated mechanistic study, *Combust. Flame* **176** (2017) 285-298. <https://doi.org/10.1016/j.combustflame.2016.10.010>

Numerical simulation of deflagration-to-detonation transition via shock-multiple flame kernels interactions

Georgios Bakalis ^a, Kelsey C. Tang-Yuk ^b, Xiaocheng Mi ^c, Nikos Nikiforakis ^c and Hoi Dick Ng ^{a†}

^a Department of Mechanical, Industrial and Aerospace Engineering, Concordia University, Montréal, QC, H3G 1M8, Canada

^b Department of Mechanical Engineering, McGill University, Montréal, QC, H3A 0C3, Canada

^c Cavendish Laboratory, Department of Physics, University of Cambridge, Cambridge, CB3 0HE, UK

[†]e-mail: hoing@encs.concordia.ca

CRediT author statement

Georgios Bakalis: Investigation, Validation, Original draft preparation. **Kelsey C. Tang-Yuk:** Investigation, Validation. **Xiaocheng Mi:** Conceptualization, Writing- Reviewing and Editing. **Nikos Nikiforakis:** Conceptualization, Resources. **Hoi Dick Ng:** Conceptualization, Writing- Reviewing and Editing, Supervision.